MRS Advances © 2020 Materials Research Society
DOI: 10.1557/adv.2020.148

Development of Dissipative Particle Dynamics framework for modeling hydrogels with degradable bonds

Vaibhav Palkar[1], Chandan K. Choudhury[1], Olga Kuksenok[1]*

[1]*Department of Materials Science and Engineering, Clemson University, Clemson, SC, 29634*

*Email: okuksen@clemson.edu

ABSTRACT

Controlled degradation of hydrogels enables several applications of these materials, including controlled drug and cell release applications and directed growth of neural networks. These applications motivate the need of a simulation framework for modeling controlled degradation in hydrogels. We develop a Dissipative Particle Dynamics (DPD) framework for hydrogel degradation. As a model hydrogel, we prepare a network formed by end-linking tetra-arm polyethylene glycol precursors. We model bond breaking during degradation of this hydrogel as a stochastic process. The fraction of degradable bonds follows first order degradation kinetics. We characterize the rate of mass loss during degradation process.

INTRODUCTION

Controlled degradation of the polymer network can be introduced in hydrogels enabling usage of these materials in a range of applications [1,2]. As an example of controlled degradation, gels with multiple degradation modes ranging between $10^{-2} – 10^{-5}$ s^{-1} have been synthesized [3] by incorporating multiple crosslinks in the polymer network. Similarly, hydrogels with multiple crosslinks which break in response to different wavelengths of light have been synthesized [4,5]. Such hydrogels can be used in selective drug [5] and cell [4] release applications. In degradation-based drug release applications, the rate of degradation reaction is essential in controlling drug release kinetics from the hydrogel [6]. This is in contrast to diffusion-based release platforms and swelling-based release platforms where the diffusion of encapsulated species and

rates of hydrogel network swelling correspondingly determine release kinetics [6]. Hydrogel degradation and subsequent drug release can be triggered as a response to external stimuli [7] such as pH [8] or light [9]. Apart from drug release applications, controlled and directed hydrogel degradation using a 2-photon laser can be utilized to develop a platform for directed growth of neural networks [2]. Existence of these systems motivates the need of a numerical framework for simulating hydrogel degradation.

Mass loss profiles from degrading hydrogels provide insights into the degradation mechanism. Bulk degradation, as opposed to surface erosion, demonstrates sudden fast mass loss due to reverse gelation of the hydrogel network [10]. Bulk degrading nanogel samples [11] and larger hydrogel samples of millimeter thickness [10] have previously been shown to exhibit fast mass loss characteristics which distinguish bulk degrading polymers from surface eroding polymers. In what follows, we will first introduce a model degradable hydrogel network and the dissipative particle dynamics (DPD) approach we use to simulate degradation process. We show that our approach reproduces first order degradation rate kinetics which corresponds to a number of experimental studies. Next, we track mass loss from bulk degrading hydrogel particles and we compare qualitative characteristics of these mass loss profiles to those observed in experimental studies.

MODEL HYDROGEL

Hydrogel networks with controlled degradation can be formed by the end-linking of two tetra-arm polyethylene glycol (tetra-PEG) precursors [12]. These networks are known to exhibit near-ideal network structure [13] and thereby show superior mechanical strength; we note, however, that the exact extent of ideality is being assessed both experimentally and theoretically [14-16]. We construct similar near-ideal tetrafunctional network as shown in Fig. 1a. This starting network structure is modeled as a diamond-like cubic lattice [17-19] with the lattice sites occupied by centers of the tetra-arm precursors. These centers are then joined by placing PEG beads (representing group of atoms in DPD framework, see below) along the direction from one center to another. The *unit cell* thus created is repeated in x, y and z directions to form the starting structure for a hydrogel particle. We refer to the hydrogels as $XxYxZ, N_x = N$ where X, Y and Z denote the number of unit cell repetitions in the x, y and z directions and N_x is the number of DPD beads within a polymer strand between junctions (see inset in Fig. 1a).

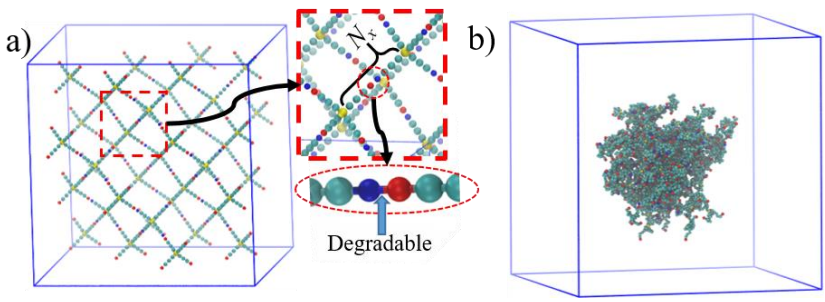

Figure 1: a) Initial structure of the model tetra-PEG network for simulations. A section of the structure marked by the red rectangle is enlarged to show tetra-arm precursors and the degradable bond. b) Snapshot of an equilibrated gel network (3x3x3, N_x=16) inside the simulation box of size 60 x 60 x 60. Beads representing water molecules are hidden for visual clarity.

The network model is nearly defect free with no elastically inactive loops but dangling ends do exist at the surface. A mere repetition of the unit cell results in formation of incomplete PEG precursors at the faces and edges of the unit cell. These incomplete precursors have a functionality less than four and are removed from the network to yield the initial gel particles. The end-linking bond between the two precursors (bond between red and blue beads in Fig. 1a) is set to be degradable. All the remaining bonds are permanent. Provided that the degradation process reaches equilibration, all the degradable bonds will be broken and only tetra-arm precursors will remain.

SIMULATION APPROACH: DISSIPATIVE PARTICLE DYNAMICS

To simulate dynamics of hydrogels, we use the dissipative particle dynamics (DPD) approach [20,21]. Individual beads in DPD represent groups of atoms. The motion of these beads is governed by Newton's equations of motion [20]:

$$\frac{d\boldsymbol{r}_i}{dt} = \boldsymbol{v}_i, \quad \frac{d\boldsymbol{p}_i}{dt} = \boldsymbol{F}_i, \tag{1}$$

where $\boldsymbol{r}_i$, $\boldsymbol{v}_i$ and $\boldsymbol{p}_i = m\boldsymbol{v}_i$ are the positions, velocities, and momenta of bead i, respectively, and $\boldsymbol{F}_i$ is the total force acting on bead i. All beads have identical mass, $m = 1$. The total force on bead i is given as $\boldsymbol{F}_i = \sum \boldsymbol{F}_{ij}^C + \boldsymbol{F}_{ij}^D + \boldsymbol{F}_{ij}^R$, where the sum is taken over other beads, j, within an interaction radius r_c. $\boldsymbol{F}_{ij}^C$ is a purely repulsive conservative force, $\boldsymbol{F}_{ij}^D$ is a dissipative, and $\boldsymbol{F}_{ij}^R$ is a random (stochastic) force. We choose the typical soft repulsion form of the conservative force:

$$\boldsymbol{F}_{ij}^C = \begin{cases} a_{ij}\left(1 - \frac{r_{ij}}{r_c}\right)\boldsymbol{e}_{ij} & (r_{ij} < r_c) \\ 0 & (r_{ij} \geq r_c) \end{cases}, \tag{2}$$

where a_{ij} is the repulsion parameter between the beads i and j, and $r_{ij} = |\boldsymbol{r}_{ij}|$ is the distance between beads i and j, with $\boldsymbol{r}_{ij} = \boldsymbol{r}_i - \boldsymbol{r}_j$, and $\boldsymbol{e}_{ij} = \boldsymbol{r}_{ij}/r_{ij}$. The repulsion parameter between different kinds of beads needs to be tuned to mimic the nature of interactions between different atoms. For interactions between the same type beads, we set $a_{ii} = 78\, k_B T/r_c$ [21]. A suitable value of the polymer-water interaction parameter (a_{pw}) can be obtained via the Flory-Huggins χ parameter as: $a_{pw} = a_{ii} + 3.27\chi$ [21]. To mimic the hydrophilicity of PEG ($\chi = 0.45$ [22], calculated $a_{pw} = 79.55$), we set $a_{pw} = 80\, k_B T/r_c$.

The random and dissipative contributions to $\boldsymbol{F}_i$ are taken as [23]:

$$\boldsymbol{F}_{ij}^D = -\gamma\omega^D(r_{ij})(\boldsymbol{e}_{ij} \cdot \boldsymbol{v}_{ij})\boldsymbol{e}_{ij}, \tag{3}$$

$$\boldsymbol{F}_{ij}^R = \sigma\omega^R(r_{ij})\zeta_{ij}\Delta t^{-1/2}\boldsymbol{e}_{ij}, \tag{4}$$

here γ and σ are the strengths of the dissipative and random forces, and $\boldsymbol{v}_{ij} = \boldsymbol{v}_i - \boldsymbol{v}_j$ is the relative bead velocity. To obey fluctuation-dissipation theorem and to ensure that the correct thermodynamic equilibrium state is reached, the following two conditions are imposed [20]:

$$\omega^D(r_{ij}) = \left[\omega^R(r_{ij})\right]^2, \qquad \sigma^2 = 2\gamma k_B T, \tag{5}$$

where k_B is the Boltzmann constant and T is the equilibrium temperature. The two conditions in eq. (5) couple the weight functions and strengths of the random and dissipative forces, respectively. We chose the weight functions in the same form as the conservative force [20]:

$$\omega^R(r_{ij}) = \begin{cases} \left(1 - \frac{r_{ij}}{r_c}\right) & (r_{ij} < r_c) \\ 0 & (r_{ij} \geq r_c) \end{cases}. \quad (6)$$

The ζ_{ij} in eq. (4) is a symmetric Gaussian random variable with zero mean and unit variance [20]. We use the harmonic potential between bonded beads in our system:

$$U_{bond} = K_b(r_{ij} - r_b)^2, \quad (7)$$

where K_b is an elastic constant and r_b is an equilibrium bond distance.

To mitigate unphysical bond crossings occurring due to the soft potential applied in our simulations, we use the modified Segmental Repulsive Potential (mSRP) [24]. Following previous studies [24], we introduce pseudo beads for all bonds in the system which are located at the center of corresponding bond. These pseudo beads interact only with other pseudo beads and the interaction force is also chosen as the soft repulsive force $\boldsymbol{F}_{ij}^{SRP} = b_{ij}(1 - r_{ij}/r_c^{SRP})\boldsymbol{e}_{ij}$. We chose $b_{ij} = 80\, k_BT/r_c$ and $r_c^{SRP} = 0.8\, r_c$ since these parameters were shown to minimize bond-crossing in the original framework [24]. The cutoff radius r_c, temperature, and a mass of a bead are set at 1.0 in reduced DPD units [20,21] and the bead number density in the simulation box is fixed at $3r_c^{-3}$. The strength of random force is chosen as $\sigma = 3$ and the time step is set at 0.02τ where τ is unit time; the unit of energy is k_BT. K_b and r_b have values of $500\, k_BTr_c^{-2}$ and $0.7r_c$ [25], respectively. The degree of coarse-graining is such that a single bead represents three water molecules [20] resulting in a dimensional value of r_c of 0.646 nm. Similarly, the dimensional unit of time can be related to the characteristic dimensionless value τ by relating diffusion coefficient of water beads, $D_{sim} = 0.17r_c^2\tau^{-1}$, with a known value of dimensional diffusion coefficient of water, D_{water}, as $\tau = 88\, ps$ [20,21]. All length and time data presented here are in reduced DPD units, r_c and τ correspondingly. To integrate dynamic equations, we use the LAMMPS simulation package [26] with mSRP code [24].

We next report simulations of hydrogel particles with different physical characteristics such as sizes and cross-link densities. The number of tetra-arm precursors and degradable bonds in a hydrogel are fixed by the number of repetitions of the initial unit cell. The 3x3x3 and 4x4x4 model networks used in this work correspondingly have 166, 423 precursors and 248, 684 degradable bonds. We then simulate gels with fixed number of unit cells and different N_x, effectively changing the crosslink density along with the hydrogel size [27]. The densely crosslinked gels are expected to have a higher elastic modulus compared to the loosely crosslinked gels [27]. A snapshot of the swollen, loosely crosslinked hydrogel particle (3x3x3, N_x=16) in water is shown in Fig. 1b. The equilibrium polymer volume fraction of these gels varies from 0.191 (for the gel with N_x=16, 3x3x3) to 0.310 (for the gel with N_x=6, 3x3x3). For the same model networks, the radius of gyration ranges between approximately 7 (for $N_x = 6$, 3x3x3) and 13 (for $N_x = 16$, 3x3x3) in reduced DPD units.

MODELING DEGRADATION

We model bond breaking during degradation as a stochastic process; this approach has been previously introduced for various reacting polymer systems [28,29]. We first set the probability of a bond breaking, P, at each reaction time step τ_r. During each time step τ_r, a random number is generated for each degradable bond; if this number is lower than P the bond is broken, otherwise the bond remains intact. Using this framework, the fraction of bonds intact, p, accurately reproduces first order degradation kinetics (Fig. 2a) with:

$$p = \frac{N(t)}{N_0} = \exp(-kt), \tag{8}$$

where $N(t)$ is the number of degradable bonds intact at any time t, N_0 is the total number of degradable bonds (i.e., number of degradable bonds at $t = 0$) and $k = P/\tau_r$ is the degradation rate constant.

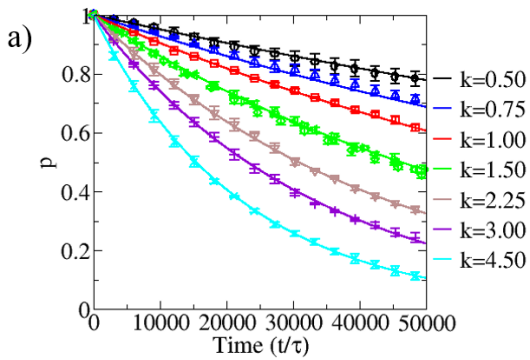

Symbol	k (units $10^{-5}\tau^{-1}$)	P	τ_R (units τ)
○	0.50	3×10^{-6}	0.6
△	0.75	3×10^{-6}	0.4
□	1.00	6×10^{-6}	0.6
◇	1.50	9×10^{-6}	0.6
◁	1.50	6×10^{-6}	0.4
▷	1.50	3×10^{-6}	0.2
▽	2.25	9×10^{-6}	0.4
+	3.00	6×10^{-6}	0.2
×	4.50	9×10^{-6}	0.2

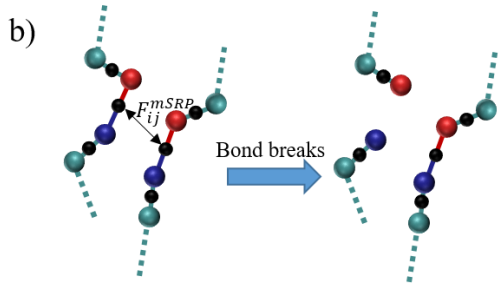

Figure 2: a) First order degradation kinetics with degradation constant that can be controlled over a range of input parameters. Symbols and solid lines represent the plots from simulations and analytical expression in Eq (8). The values of k, P and τ_R are listed in the legend. Error bars indicate standard deviation over three simulations. b) Schematic of the bond breaking mechanism. When a bond breaks, the corresponding pseudo bead used in mSRP (black bead in schematic) is deleted from the simulation.

Thus, the degradation rate k can be controlled by varying the input parameters, P and τ_r. We first performed simulations of a 4x4x4, $N_x = 6$ hydrogel in a $13 \times 13 \times 13$ simulation box with a range of values of P and τ_r. The data from these simulations is summarized in Fig. 2a which demonstrates that this framework provides access to a range of degradation rates. Note that, as anticipated, deviations from the analytical estimates are somewhat higher at higher τ_r (deviations of mean and larger error bars for black and blue data sets in Fig. 2a for $\tau_r = 0.6\tau$ and $\tau_r = 0.4\tau$, respectively). Thus, we chose $\tau_r = 0.2\tau$ in simulations below which is 10 times the DPD time step. Another important aspect in the choice of parameters is the comparison of hydrogel degradation with the diffusion of water molecules. The degradation rate constant k for our reference parameter set ($P = 3 \times 10^{-6}$, $\tau_r = 0.2\tau$) results in characteristic degradation time of $10^5\tau$. Water diffusion over the average length of a polymer strand taken for simplicity as $5r_c$ occurs much faster; relaxation time of water molecule diffusion is estimated as 10τ using $D_{sim} = 0.17\, r_c^2\tau^{-1}$. Thus, water diffusion is $O(10^4)$ faster as compared to degradation process.

Special care is needed in using the mSRP between the bonds. As discussed in the simulation approach section, a pseudo bead is introduced for each of the bonds. In the

degradation framework of hydrogel, when a bond breaks, the corresponding pseudo bead loses its identity and must be deleted to prevent introduction of unphysical interactions. The schematic in Fig. 2b illustrates such deletion of the pseudo beads. We implemented this deletion in the mSRP code of LAMMPS simulation package. As a bond breaking event occurs, all pseudo beads are deleted and new pseudo beads are created only for the bonds still intact in the simulation.

We now demonstrate the application of the above degradation framework to single gel particles. First, we make two hydrogel networks with 3x3x3 repetitions and N_x=6 and N_x=16, respectively. These gels have a total mass of m_0=2158 and, 5478, respectively, in reduced DPD units. These networks are first equilibrated in water (see snapshots in Fig. 3a,e) and subsequently degraded (snapshots in Fig. 3b-d,f-h).

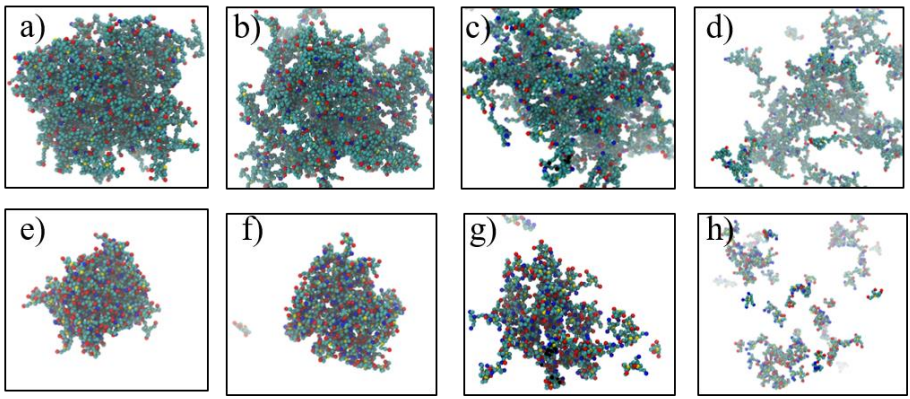

Figure 3: Snapshots during degradation of (a-d) a 3x3x3, N_x=16 and (e-h) a 3x3x3, N_x=6 gel. (a,e) Equilibrium snapshots prior to degradation and, at (b,f) t=10,000, (c,g) t=30,000, (d,h) t=50,000 after starting degradation. Here, we set $k = 1.5\text{x}10^{-5}\tau^{-1}$. Quantitative mass loss data for these simulations is presented in Fig. 4a.

When the degradation is switched on, mimicking the application of an external degradation stimulus (for example light), gels first undergo erosion and fragments with the single tetra-arm precursors start leaving the gel particles. We characterize degradation of these fragments via the fractional mass loss from the intact original gel particle (Fig. 4a). To measure this mass loss, we first define clusters as sets of bonded beads in the system. We then define our degrading gel particle to be the largest such cluster (cluster with highest number of beads) and measure the mass of this largest cluster (m(t)). The fractional mass loss is then measured as the difference between the mass of this cluster and the mass of hydrogel particle normalized by the mass of the original particle ($(m_0 - m(t))/m_0$). During the initial stages of degradation, only smaller fragments are eroded from the gel resulting in short vertical jumps in the mass loss data shown in Fig. 4a. At later stages, the gel loses larger fragments consisting of several tetra-arm precursors (see snapshots in Fig. 3). This results in sudden large mass losses, shown by the larger vertical jumps in the data of Fig. 4a.

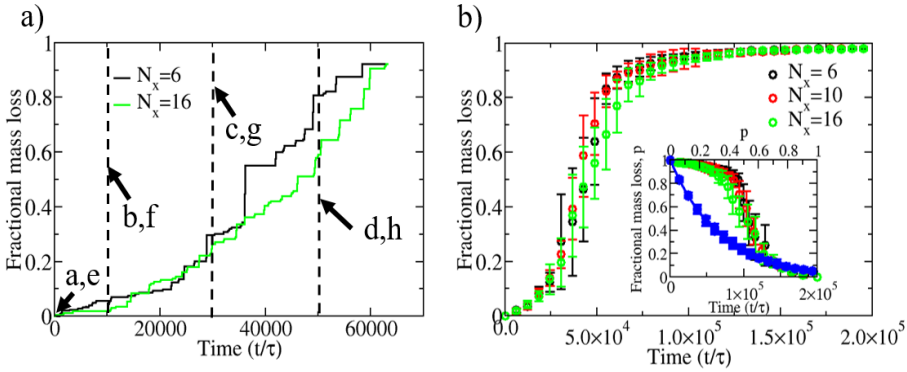

Figure 4: a) Mass loss data for 3x3x3, N_x=6 and 3x3x3, N_x=16 gels. Dashed lines indicate time instances corresponding to the snapshots in Fig. 3. b) Mass loss data for 3x3x3 gels with N_x=6,10,16 averaged over 8 independent simulations each. Error bars indicate standard deviation. Inset: red, green and black symbols – fractional mass loss as a function of p (top x axis), the colors are the same as in the legend in the main plot; and blue symbols – p as a function of time (bottom x-axis).

In the next series of simulations, we analyzed degradation process of the 3x3x3 gels with $N_x = 6,10,16$. Eight independent runs were performed for each of these gels (Fig. 4b). The number of precursors and the number of the degradable bonds remains constant in three cases shown in Fig. 4b, however, the size of each precursor increases and crosslink density decreases with an increase in N_x. As anticipated based on results in Fig. 2, all hydrogels follow the same first-order bond breaking kinetics (see blue symbols in the inset of Fig. 4b that represent the data for all the gel samples shown in main plot (all runs), with the solid blue line representing the analytical curve, eq. (8)). Further, all three model gels exhibit close trends in fractional mass loss, with somewhat slower mass loss for the gels with N_x=16. In all the cases, fractional mass loss shows an initial slow mass loss regime where only small fragments leave the hydrogel. This regime is followed by a faster mass loss caused by breaking off of large fragments and disintegration of the network for all the cases considered. These are features of erosion and reverse gelation observed in previous experimental studies [10]. We note that the bulk degrading polymers have been shown to exhibit distinctly different mass loss kinetics compared to kinetics of bond breaking [31]. Our simulation results (inset of Fig. 4b) also demonstrate this trend. Thus, our results show that the fractional mass loss primarily depends on the degradation rate constant and a number of degradable bonds (or a number of precursors) and follows similar trends for the gels with different crosslink densities.

CONCLUSIONS

We have developed a DPD framework for modeling degradation of hydrogels. Using this framework, degradation can be tracked via the fraction of degradable bonds intact which displays first order degradation kinetics. The first order kinetics of bond degradation is consistent with several experimental studies [6,12,30] thus our framework is expected to be applicable to a range of systems. We also characterize degradation by tracking fractional mass loss from the hydrogel. Our results show that an initial slow mass loss regime where only small fragments leave the hydrogel is followed by a faster

mass loss regime caused by the disintegration of the bulk network, which is consistent with prior experimental observations.

ACKNOWLEDGMENTS

O.K. gratefully acknowledges partial support of National Science Foundation EPSCoR Program Award No. OIA-1655740, and partial support of NSF MRI Award No. 1725573. Clemson University is acknowledged for compute time on Palmetto cluster.

REFERENCES

1. M. A. Azagarsamy, D. D. McKinnon, D. L. Age and K. S. Anseth, ACS Macro Lett. **3** (6), 515-519 (2014).
2. D. D. McKinnon, T. E. Brown, K. A. Kyburz, E. Kiyotake and K. S. Anseth, Biomacromolecules **15** (7), 2808-2816 (2014).
3. P. M. Kharkar, K. L. Kiick and A. M. Kloxin, Polym. Chem. **6** (31), 5565-5574 (2015).
4. V. X. Truong, F. Y. Li and J. S. Forsythe, ACS Appl. Mater. Interfaces **9** (38), 32441-32445 (2017).
5. D. R. Griffin and A. M. Kasko, ACS Macro Lett. **1** (11), 1330-1334 (2012).
6. C. C. Lin, and A. T. Metters, Adv. Drug Delivery Rev. **58** (12-13), 1379-1408 (2006).
7. J. Li and D. J. Mooney, Nature Reviews Materials **1** (12), 1-17 (2016).
8. Y. Zhang, R. Wang, Y. Hua, R. Baumgartner, and J. Cheng, ACS Macro Letters, **3** (7), 693-697 (2014).
9. M. W. Tibbitt, B. W. Han, A. M. Kloxin, and K. S. Anseth, J. of Biomed. Mat. Res. Part A, **100** (7), 1647 (2012).
10. A. T. Metters, C. N. Bowman, and K. S. Anseth, The Journal of Physical Chemistry B, **104** (30), 7043-7049 (2000).
11. Z. Stillman, B. M. Jarai, N. Raman, P. Patel, and C. A. Fromen, Polymer Chemistry, **11** (2), 568-580 (2020).
12. X. Li, Y. Tsutsui, T. Matsunaga, M. Shibayama, U. Chung and T. Sakai, Macromolecules **44** (9), 3567-3571 (2011).
13. T. Sakai, T. Matsunaga, Y. Yamamoto, C. Ito, R. Yoshida, S. Suzuki, N. Sasaki, M. Shibayama and U. I. Chung, Macromolecules **41** (14), 5379-5384 (2008).
14. T. S. Lin, R. Wang, J. A. Johnson and B. D. Olsen, Macromolecules **51** (3), 1224-1231 (2018).
15. F. Lange, K. Schwenke, M. Kurakazu, Y. Akagi, U. I. Chung, M. Lang, J. U. Sommer, T. Sakai and K. Saalwachter, Macromolecules **44** (24), 9666-9674 (2011).
16. K. Schwenke, M. Lang and J. U. Sommer, Macromolecules **44** (23), 9464-9472 (2011).
17. L. Comić and B. Nagy, Acta Crystallographica Section A: Foundations and Advances **72**(5), 570-581 (2016).
18. P. K. Jha, J. W. Zwanikken, F. A. Detcheverry, J. J. De Pablo and M. O. de la Cruz, Soft Matter **7** (13), 5965-5975 (2011).
19. X. Yong, O. Kuksenok, K. Matyjaszewski and A. C. Balazs, Nano Letters **13** (12), 6269-6274 (2013).
20. R. D. Groot and P. B. Warren, J. Chem. Phys. **107** (11), 4423-4435 (1997).
21. R. D. Groot and K. L. Rabone, Biophys. J. **81** (2), 725-736 (2001).
22. A. T. Metters and J. A. Hubbell, Biomacromolecules **6** (1), 290-301 (2005.).
23. P. Español and P. B. Warren, J. Chem. Phys. **146** (15), 150901 (2017).
24. T. W. Sirk, Y. R. Slizoberg, J. K. Brennan, M. Lisal and J. W. Andzelm, J. Chem. Phys. **136** (13), 11 (2012).
25. C. K. Choudhury and O. Kuksenok, MRS Advances **3** (26), 1469-1474 (2018).
26. S. Plimpton, J. Comput. Phys. **117** (1), 1-19 (1995). URL: https://lammps.sandia.gov/index.html
27. C. K. Choudhury, V. Palkar, and O. Kuksenok, Langmuir (2020) doi:10.1021/acs.langmuir.9b03486.
28. R. L. C. Akkermans, S. Toxvaerd and W. J. Briels, J. Chem. Phys. **109** (7), 2929-2940(1998).
29. A. Milchev, J. P. Wittmer and D. P. Landau, J. Chem. Phys. **112** (3), 1606-1615 (2000).
30. T. E. Brown, I. A. Marozas and K. S. Anseth, Adv. Mater. **29** (11), 7 (2017).
31. A. Gopferich, Macromolecules **30** (9), 2598-2604 (1997).